Target localization using TDoA measurement and accelerometer sensor with unknown propagation speed

Ajib Setyo Arifin and Teguh Samudra Firdaus

Department of Electrical Engineering, Universitas Indonesia, Indonesia
ajib@eng.ui.ac.id; samudraasta@gmail.com

Abstract: Target detection on the surface of water using wireless sensor networks (WSNs) should be able to collect information as much as possible. The previous studies are only able to collect speed and direction of the target. In addition to previous studies, we collect not only speed and direction but also real time location of the target. In this paper, we propose a target localization algorithm based on Time Different of Arrival (TDoA). The proposed algorithm takes into account grid topology of sensors because it is more tractable. The algorithm is validated using experiments to compute the mean average error (MAE); in these experiments, the estimated and real location coordinates were compared. The experimental results achieved the smallest MAE at 0.25 m. The experimental results indicated that the MAE is inversely proportional to the distance between the sensors. Moreover, the MAE of the x-axis is always greater than that of the y-axis is well explained using the principle of the Abbe error.

Keywords: Target localization; TDoA, accelerometer, Mean average error (MAE); Wireless sensor network (WSN)

1. Introduction

Wireless sensor network (WSN), which consists of sensors with sensing, computing, and communication capabilities, has broad applications, including industrial monitoring, structural health monitoring, agriculture monitoring, landslides monitoring, and marine monitoring [1]–[6]. From the perspective of the authorities, monitoring systems can be classified as cooperative and intrusive. A cooperative monitoring system is one in which the targets cooperatively broadcast their identity, such as in an automatic identification system (AIS). Conversely, an intrusive monitoring system is one in which targets are monitored with or without their knowledge. In terms of protecting marine resources and preventing illegal activities, an intrusive monitoring system is more suitable. Conventional intrusive monitoring systems use radar or satellites, which are very expensive to construct and operate. In addition to being expensive, optical satellite imagery can be covered in clouds, and marine radar imagery is susceptible to noise or clutter from surface waves [7].

Received: September 30th, 2022. Accepted: December 30th, 2023

DOI: 10.15676/ijeei.2023.15.4.9

There is much recent research for intrusive monitoring using WSN. Sharma et al. proposed a three-level hierarchy-based sensor network to detect a mobile target using static acoustic sensors and a sensing probability model [8]. They used k-mean clustering and Likelihood Ratio Test (LRT) to minimize false alarms and maximize detection probability. The development of anti-reconnaissance technology in which the target can avoid its detection brings new challenges. To solve this problem, Wang et al. proposed a collaboration model in which static sensors and mobile sensing vehicles cooperate to provide intrusive detection against the target [9]. They used a target pursuit algorithm and a sleep-scheduling strategy for the mobile sensing vehicles and the static sensors, respectively. Mahopatra et al. proposed a big data architecture to process and studied the enormous volume of data produced by static camera sensors to detect the intrusive target [10]. Wang et al. studied a binary sensing model in which a sensor used only 1-bit information regarding the target presence or absence. They proposed a tracking algorithm to estimate the target's location, velocity, and trajectory [11]. Arik et al. proposed a Collaborative Mobile Target Imaging (CMTI) algorithm using radar sensors to detect, track, and image the targets [12]. Intrusive target detection that uses any type of sensors, including magnetometers, thermal sensors, or acoustic sensors was investigated in [8], [13]–[15]. Moreover, Arora et al. and Duarte et al. successfully deployed target detection and classification in real-world systems [16], [17]. However, most research is conducted using static sensors after deployment and may work well on the land. Intrusive monitoring in a watery environment differs in many aspects. The main challenge is that when the sensors are deployed on the sea surface, they are not static and get tossed by sea waves that make them move around randomly.

There are several papers for intrusive monitoring using WSN in the watery environments. Bunin et al. experimented ship detection for tracking and classification on the Hudson River Estuary [18]. They used a video system and an underwater acoustic sensor on the river. Carapezza et al. proposed a coastal sensor network for detection, classification, and tracking sub-merge object. They refined tracking on the targets using shore-based optical sensors [19]. However, these are shore-based detection systems. In addition to shore-based detection, offshore-based detection has been investigated in [20]–[23]. Kdouh et al. researched object monitoring onboard ships using Zigbee-based equipment [20]. The paper studied the possibility of replacing wired connections into wireless. The result showed that the wireless solution could be a cost-effective alternative to wired connections. However, intrusive monitoring was not part of their research. Luo et al. proposed an intrusive ship detection by distinguishing the ship-generated waves from the ocean waves [21]. They designed a three-tier intrusive detection system by taking spatial and temporal correlations into account to increase detection reliability. Equipped with three-axis accelerometer sensors, they estimated the ship’s velocity and detection latency. They also proposed a novel floating three-dimensional sensors to enlarge the monitoring area [22]. However, the ship location estimation has not been considered yet. Rao et al. proposed an intrusive ship detection algorithm to classify and locate the ship [23]. A waveform classification algorithm was proposed to distinguish various objects by the waveform patterns generated by a group of sensor nodes. Moreover, they also proposed a target location estimation that was simply assumed the same as the sensor nodes' location at a certain time. This method can cause inaccurate location detection since the ship's real location may differ from the location of the representative sensor node. The error location detection can get worsen if the distance of the sensing radius and sensor is large. Therefore, improvement of location detection is important. In this paper, we proposed a target localization using Time Difference of Arrival (TDoA) measurements from accelerometer-based sensors. We derived a closed-form expression of the target location formulation by considering the grid-based sensor deployment. We validated our proposed formulation by conducting real world experiment. We developed a detection system consisting of sensor nodes, transceiver modules, and a personal computer (PC) to support the proposed formulation. The functions of the sensor nodes were to observe, process, and send the information obtained with the aid of software. Moreover, the information sent by the sensor nodes was received by the transceiver module connected to the PC. The software that implemented the proposed target location formulation was installed in the PC for the target location. The experiment was designed to determine the accuracy of the target location using the proposed algorithm. The accuracy was calculated using the mean average error (MAE) by comparing the actual and estimated target locations. MAE was calculated using several variables, such as distance between sensor, error speed, and direction. The smallest MAE was obtained at 0.25 m when the distance between sensors was 2 m. These results indicated that the proposed target location estimation algorithm can be the basis for the development of determining target locations based on a WSN.

The remainder of this paper is organized as follows. In Section 2, we review the related works. In Section 3, the derivation of the target location is presented. In Section 4, the design of the location detection system consisting of hardware and software is described sequentially. Section 5 describes the experimental procedures. Sections 6 and 7 present the experimental results and discussion, respectively. Section 8 presents the conclusion.

2. Related Work

Target localization is a hot topic in WSN. Souza et al. conducted an excellence survey in target localization for WSN [24]. There are four steps to obtain the target location: sensor localization, target detection, sensor collaboration, and target position computation.

The sensor location information is used to be a reference of the target location [25]. In general the sensor location information is taken from how the sensors are deployed: strategic or random [26]–[28]. The strategic sensor deployment can be optimally determined the sensor location to minimize the target location error [29], [30] [31]–[33]. On the other hand, the random sensor deployment can be categorized into range-based and range-free-based [34]. Range-based localization uses radio propagation characteristics including Angle of Arrival (AOA) [35], Time of Arrival (ToA) [36], TDoA [37], Received Signal Strength (RSS) [38], [39], and Doppler-based [40], [41] to determine unknown sensor location from the beacon sensor. Range-free-based localization known as hop-count-based localization uses the average hop distance to approximate the actual distances [42].

Target detection defines an event when sensor readings match the conditions that describe the target . How the sensor reading signals from the target depends on type of sensor data and matching techniques [43], [44]. The types of sensor data include accelerometer, acoustic, seismic, infrared, radio frequency identification (RFID), light, radar, image, and video data [21], [44]–[48]. The each types of sensor data requires different types of matching techniques. A sensor node detects the present of the target when the sensor data exceed a predetermined threshold such as energy level, frequency spectrum, weight level, speed level, light intensity, pixel metrics, and image pattern.

Sensor collaboration defines how communication between sensors occur when an event is detected [49], [50]. In general, there are two methods: centralized and decentralized. The centralized method defines the sensor nodes that detect the target and send their data toward the sink node. This method is simple with expense of possible network congestion as the number of receive messages increases at the sink node [51]. To overcome the network congestion, the decentralized method was proposed by sending only a single data report to the sink from a group of sensors [52]. This method requires a node as a cluster head that responsible for fusion and transmission of the data to the sink node [53]. The cluster nodes usually deplete their power faster than others. Because of unavailable the direct hop, data transmission requires a complex routing protocol.

The target position computation refers to find the distance and the position of the target relative to the sensor location [54]. Some sensor localization methods can be directly applied including RSS and TDoA to calculate the distance. However, these techniques demand a constant propagation speed of the signal emitted by the target [55]. Moreover, the computation method of the target position can use trilateration, multilateration, and bounding box that are non-convex problem [56], [57].

In this work, we used the grid-based sensor deployment for more tractable modeling. The target detection used accelerometer-based sensor for harsh environment [21], [58]. The sensor performed an energy level matching to detect the present of the target. We chose the centralized method for sensor collaboration since it has less complex network structure than the decentralized method. The existing methods for the target position computation demanded a known propagation speed of the target-generated waves. However, since the speed of the water waves was not constant, distance computation became difficult. To solve that problem, we proposed a distance formulation using TDoA-based measurement with unknown propagation speed. Moreover, the position computation was simply derived using Trigonometry in a closed-form expression.

3. Derivation Of Target Location Formulation

To calculate the coordinates of the target location, we derived the proposed algorithm from the grid-shaped modeling of sensor placement. Grid modeling was first used by Lou et al. [21]. Grid modeling was selected because the results of the formulation were more tractable than random modeling. In this model, four sensors, $s_1 - s_4$, are arranged in a rectangular formation with the length of the sides, L (Figure 1).

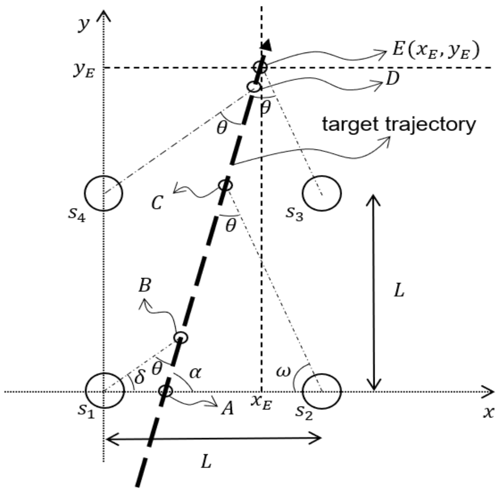

Figure 1. Grid model of the target location detection system.

The moving target cleaves the sensor formation by direction (α) and sequentially through points $A, B, C, D,$ and E. The point A is the point of intersection between the horizontal axes and the target path. The points $B, C, D,$ and E are the points of intersection of the target path with the target's diverging wave line to sensors s_1, s_2, s_3, and s_4, respectively. The diverging waves are waves with a V pattern that are formed by two loci of cusps whose angle with the sailing line is $\theta = 19^0 28'$ in deep water [44]. For this point $E(x_E, y_E)$, the target coordinates can be calculated using the following steps:

A. Compute Distance $s_1 A$

Using the principle of trigonometry, the comparison between $s_1 A$ and AB can be expressed as

$$\frac{s_1 A}{\sin\theta} = \frac{AB}{\sin\delta} \tag{1}$$

$$s_1A = \frac{AB \sin\theta}{\sin\delta}.$$

Moreover, As_2 can be expressed as

$$As_2 = \frac{AC \sin\theta}{\sin\omega}. \tag{2}$$

Using (1) and (2), the comparison of s_1A and As_2 can be computed as

$$\frac{s_1A}{As_2} = \frac{AB \sin\omega}{AC \sin\delta} \tag{3}$$

Because the total number of angles in a triangle is 180^0 and $\theta = 19^0 28'$, ω and δ can be expressed as a function of α; therefore, (3) can be obtained as

$$\frac{s_1A}{As_2} = \frac{AB \sin\omega}{AC \sin\delta}$$

$$= \frac{AB \sin(160^0 32' - \alpha)}{AC \sin(\alpha - 19^0 28')}. \tag{4}$$

The estimated direction of the moving target was formulated from [1] is

$$\alpha = \tan^{-1}\left(\frac{t_{s_3} + t_{s_4} - t_{s_1} - t_{s_2}}{t_{s_1} + t_{s_2} - t_{s_3} - t_{s_4}} \tan 70^0\right). \tag{5}$$

where t_{s_i} is a timestamp at which the diverging waves intrude the i-th sensor.

The comparison between s_1A and As_2 is also affected by the comparison of the timestamp in the first and second sensors, which enables three conditions, i.e., $t_{s_1} < t_{s_2}$, $t_{s_1} = t_{s_2}$, and $t_{s_1} > t_{s_2}$ (Figure 2). The condition $t_{s_1} < t_{s_2}$ occurs when the diverging waves hit the first sensor before the second sensor. The condition $t_{s_1} = t_{s_2}$ occurs when the diverging waves hit the first and second sensors simultaneously. The condition $t_{s_1} > t_{s_2}$ occurs when the diverging waves hit the second sensor before the first sensor.

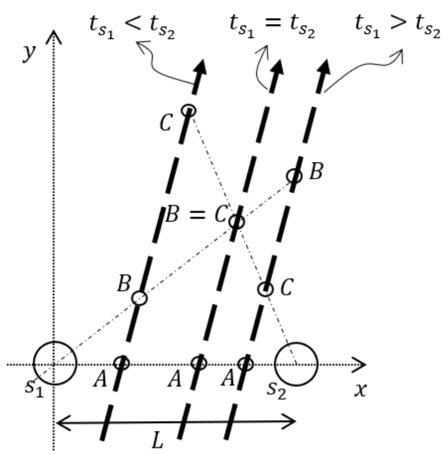

Figure 2. Three conditions of the timestamp between first and second sensors, i.e., $t_{s_1} < t_{s_2}$, $t_{s_1} = t_{s_2}$, and $t_{s_1} > t_{s_2}$.

A.1. Condition $t_{s_1} < t_{s_2}$

s_1A can be calculated by first computing BC as

$$BC = v(t_{s_2} - t_{s_1}). \tag{6}$$

where v is the estimated speed of the target as a function of L and α [1]:

$$v = \frac{L \quad \sin(\alpha + 70^0)}{\left(t_{s_4} - t_{s_1}\right) \sin 19^0 28'}. \tag{7}$$

Given $FB,$ which is parallel to s_2C (Figure 3), Fs_2 can be computed using the principle of trigonometry as follows:

$$\frac{Fs_2}{\sin\omega} = \frac{BC}{\sin\theta}$$

$$Fs_2 = \frac{BC \sin\omega}{\sin\theta}$$

$$= \frac{BC \sin(160^0 32' - \alpha)}{\sin 19^0 28'}. \tag{8}$$

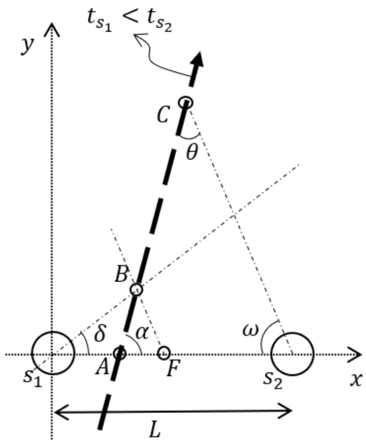

Figure 3. Condition $t_{s_1} < t_{s_2}$.

Figure 3 indicates that

$$s_1A + AF = L - Fs_2$$

$$AF = L - Fs_2 - s_1A. \tag{9}$$

Using the principle of trigonometry, the comparison between s_1A and AF can be expressed as

$$\frac{s_1A}{\sin\omega} = \frac{AF}{\sin\delta}$$

$$s_1A = AF\frac{\sin\omega}{\sin\delta}. \tag{10}$$

Substituting (6), (8), and (9) into (10), s_1A can be expressed as

$$s_1A = \frac{\sin\omega}{\sin\omega + \sin\delta}(L - Fs_2)$$
$$= \frac{\sin(160^0 32' - \alpha)}{\sin(160^0 32' - \alpha) + \sin(\alpha - 19^0 28')}\left(L - \frac{v(t_{s_2} - t_{s_1})\sin(160^0 32' - \alpha)}{\sin 19^0 28'}\right). \quad (11)$$

A.2. Condition $t_{s_1} = t_{s_2}$

This condition is such that $AB = AC$ (Figure 4).

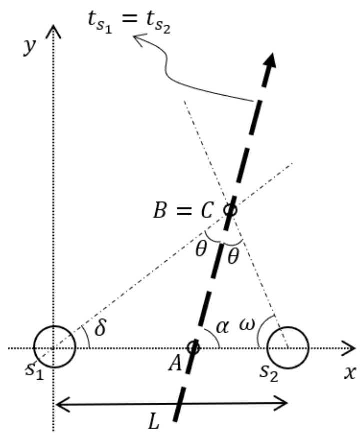

Figure 4. Condition $t_{s_1} = t_{s_2}$.

The length s_1A can be derived from the comparison of ω and. δ

$$\frac{s_1A}{\sin\omega} = \frac{As_2}{\sin\delta}$$

$$s_1A = \frac{As_2 \ \sin\omega}{\sin\delta}. \quad (12)$$

With the aid of $L = s_1A + As_2$, $\omega = \ 160^0 32' - \alpha$, and $\delta = \alpha - 19^0 28'$, (12) can be expressed as

$$s_1A = \frac{L\sin(160^0 32' - \alpha)}{\sin(160^0 32' - \alpha) + \sin(\alpha - 19^0 28')}. \quad (13)$$

A.3. Condition $t_{s_1} > t_{s_2}$

With the aid of *GC*, which is parallel to s_1B (Figure 5), the length s_1A can be expressed as $s_1A = s_1G + GA$. Furthermore, to compute s_1G, CB must be computed as follows:

$$CB = v(t_{s_1} - t_{s_2}). \quad (14)$$

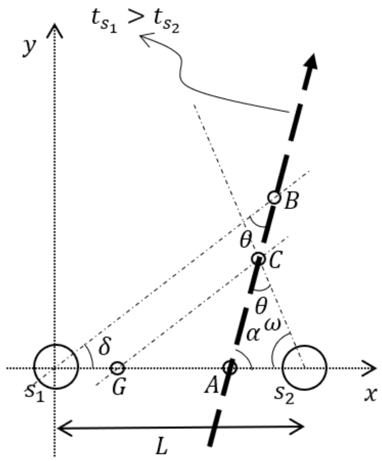

Figure 5. Condition $t_{s_1} > t_{s_2}$.

Using the length CB, s_1G can be computed as

$$s_1G = \frac{CB \sin\theta}{\sin\delta}$$

$$= \frac{v(t_{s_1} - t_{s_2}) \sin(19^0 28')}{\sin(\alpha - 19^0 28')}. \tag{15}$$

From Figure 5, the comparison between GA and As_2 with their angles, δ and ω, can be expressed as

$$GA = \frac{As_2 \sin\omega}{\sin\delta}.$$

$$= \frac{As_2 \sin(160^0 32' - \alpha)}{\sin(\alpha - 19^0 28')}. \tag{16}$$

From Figure 5, the length As_2 can be obtained using the following expression:

$$As_2 = L - s_1G - GA.$$

$$= L - . \frac{v\left(t_{s_1} - t_{s_2}\right) \sin(19^0 28')}{\sin(\alpha - 19^0 28')} - GA. \tag{17}$$

Substituting (17) into (16), the length GA can be formulated as

$$GA = \left(L - \frac{v(t_{s_1} - t_{s_2}) \sin(19^0 28')}{\sin(\alpha - 19^0 28')}\right) \frac{\sin(160^0 32' - \alpha)}{\sin(160^0 32' - \alpha) + \sin(\alpha - 19^0 28')}. \tag{18}$$

Finally, the length s_1A at the condition $t_{s_1} > t_{s_2}$ can be expressed as

$$s_1A$$

$$= \frac{v(t_{s_1} - t_{s_2}) \sin(19^0 28')}{\sin(\alpha - 19^0 28')}$$

$$+ \left(L - \frac{v(t_{s_1} - t_{s_2}) \sin(19^0 28')}{\sin(\alpha - 19^0 28')}\right) \frac{\sin(160^0 32' - \alpha)}{\sin(160^0 32' - \alpha) + \sin(\alpha - 19^0 28')}. \tag{19}$$

B. Computing AE

The requirements for calculating the length AE are that the timestamp of the third sensor should be greater than or equal to that of the fourth sensor, $t_3 \geq t_4$. From Figure 1, AE can be expressed as

$$AE = AB + BE, \tag{20}$$

where

$$AB = \frac{s_1A \quad \sin\delta}{\sin\theta}$$

$$= \frac{s_1A\sin(\alpha - 19^0 28')}{\sin(19^0 28')}, \tag{21}$$

and BE is the product of the target speed and the difference in timestamps between the third and first sensors:

$$BE = v(t_3 - t_1). \tag{22}$$

B.1. Computing s_1x_E

From Figure 1, the length s_1x_E can be expressed as

$$s_1x_E = s_1A + Ax_E, \tag{23}$$

where the length s_1A can be computed using (11), (13), or (19) depending on the timestamp comparison between the first and second sensors. Using (20)–(22), the length Ax_E can be formulated as

$$Ax_E = AE\cos\alpha$$

$$= \left(\frac{s_1A\sin(\alpha - 19^0 28')}{\sin(19^0 28')} + v(t_3 - t_1)\right)\cos\alpha. \tag{24}$$

B.2. Computing s_1y_E

The length s_1y_E is equal to x_EE:

$$s_1y_E = x_EE$$

$$= AE\cos(90 - \alpha)$$

$$= \left(\frac{s_1A\sin(\alpha - 19^0 28')}{\sin(19^0 28')} + v(t_3 - t_1)\right)\cos(90 - \alpha). \tag{25}$$

Assuming that the first sensor is located at the origin (0, 0), the coordinate $E(x_E, y_E)$ can be expressed as $E(s_1x_E, s_1y_E)$ based on (24) and (25).

C. Computing AD

The computation of the length AE using (20) is only valid for $t_3 \geq t_4$, while for $t_3 < t_4$, AE is replaced by, AD (Figure 6). Moreover, AD can be expressed simply as

$$AD = AB + BD, \tag{26}$$

where AB can be obtained from (21) and BD is the product of the target's speed (v) and the difference of the timestamps of the fourth and first sensors:

$$BD = v(t_4 - t_1). \tag{27}$$

C.1. Computing s_1x_D

From Figure 6, the length s_1x_D can be computed as

$$s_1x_D = \mathrm{s}_1A + Ax_D, \tag{28}$$

where the length s_1A can be obtained using (11), (13), and (19). The length Ax_D is computed using

$$Ax_D = AD\cos\alpha, \tag{29}$$

where AD is computed from (26).

C.2. Computing s_1y_D

The length s_1y_D can be expressed as

$$s_1y_D = AD\cos(90 - \alpha), \tag{30}$$

where AD is obtained from (26).

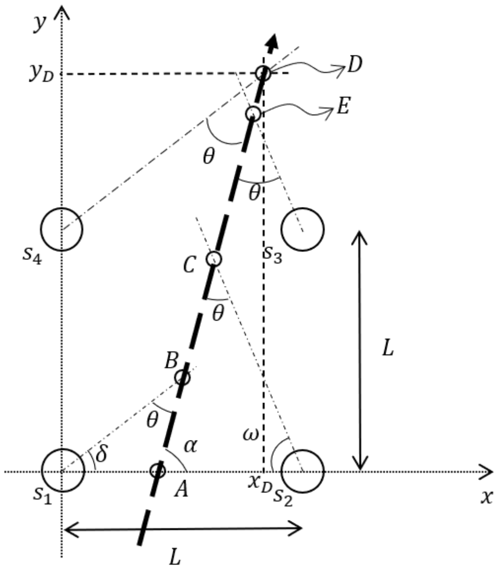

Figure 6. Condition $t_3 < t_4$.

In summary, the target coordinates can be calculated from the input parameters consisting of the distance between sensors (L) the target's speed (v) and the target's direction (α).

4. Target Detection System

The detection system consisted of three main components: the target, sensors, and PC. The target traveling at v produced wave ripples. These waves were captured by an accelerometer on each sensor. If the signal produced by the accelerometer was greater than or equal to a threshold signal, each sensor stored the timestamp of the arrival of the wave ripples. The timestamp data were sent to the PC wirelessly using an XBee S2 transceiver module. To receive signals from the sensors, the PC was equipped with an XBee Explorer module through a universal serial bus (USB) cable. When the PC obtained signals from the four sensors, the software calculated the approximate location of the target in the x and y coordinates using the algorithm in Section 3.

A. Hardware

The hardware consisted of four sensors and a PC. The term sensor means that a device consisted of an Arduino Uno R3 controller, an accelerometer, an XBee S2 transceiver module, and a Li-Ion 18650 battery (Figure 7). These devices were assembled in a box for easy mounting with a buoy. The Windows-based PC and Xbee Explorer were used to operate software that was designed for the system. The hardware architecture is shown in Figure 7.

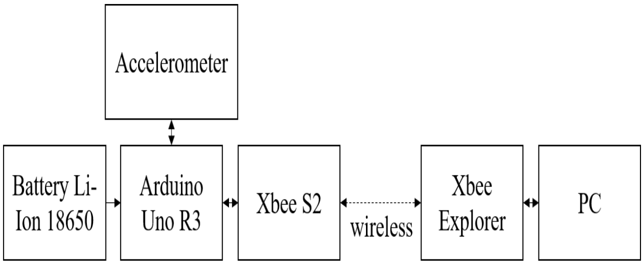

Figure 7. Hardware architecture.

B. Software

The software was used to process information in the sensor and PC. The software in the sensor was designed using the Arduino Integrated Development Environment (IDE) based on the C and C++ programming languages. This software was in charge of detecting signals from moving targets. If the received signal exceeded or equaled the threshold, the timestamp would be recorded and sent to the PC. The threshold was the minimum signal value from the accelerometer, which indicated a moving target. The threshold value was obtained from the training data generated from the experiment. The software algorithm is shown in Algorithm 1.

Algorithm 1 Sensor-tier Detection Algorithm

1: **Initialization**: switch sensor on, set threshold.

2: **Ouput**: timestamp

3: **Loop for** signal observation

4: Sensor samples signal from accelerometer every 28 ms.

5: **If** the sample signal $\geq$ threshold

6: **do** record and send timestamp

7: **end**.

The software installed on the PC was designed using a processing IDE based on the Java programming language. When the PC received the timestamp from the four sensors, the software calculated the x and y coordinates of the location of the moving target. The software algorithm is shown in Algorithm 2.

Algorithm 2 Cluster-tier Detection Algorithm

1: **Initialization**: set L, $\theta = 19^0 28'$

2: **Output**: x and y coordinates

3: **Loop for** listening for timestamp from sensor 1st, 2nd, 3rd, and 4th.

4: **If** the timestamp complete?

5: **do** compute x and y coordinates as location of the target using steps in Section 2

6: **end**

5. Experimental Procedure

The purpose of this experiment was to validate the proposed method by calculating the MAE for the x-axis, which can be expressed as

$$\mathrm{MAE}_x = \frac{1}{N}\sum_{i=1}^{N}|x_i - \hat{x}|, \tag{31}$$

where x_i is the length of the x-axis as the result of computation using (23) or (28) in the i-th experiment, $\hat{x}$ is the length of the x-axis from the measurement, and N is the number of experiments. To compute the MAE for the y-axis, (31) can be used by changing x into y as follows:

$$\mathrm{MAE}_y = \frac{1}{N}\sum_{i=1}^{N}|y_i - \hat{y}|, \tag{32}$$

where y_i is the length of the y-axis as the result of computation using (25) or (30) in the i-th experiment, And $\hat{y}$ is the length of the y-axis from the measurement.

The experiment was conducted in a pool with a relatively calm water surface to minimize noise generated from wave ripples other than the target ripples. To ensure that the sensors did not move, we tied them using ballasts (Figure 8). Furthermore, a toy ship was used as the moving target, and it passed by all four sensors N-times with constant v and α. The target was pulled by a rope wound on an electric motor with constant rotation to maintain a constant speed and direction. The experiment was conducted by varying L, v, and α. Moreover, before collecting location detection data, the threshold data is required to be obtained first. Subsequently, the threshold data were used in the software in the sensor module described in Section 4.2.

The length estimation of x and y was a function of L, v, and α, where v and α tended to have errors as in. The error in v and α may have propagated into the estimation of x and y. Therefore, to observe and reduce the propagation errors, the experiment was conducted with three scenarios: the first was an experiment without error control, and all the estimated values of v and α were used as inputs to estimate the lengths of x and y. The second was an experiment with speed control errors, and only the value of v that satisfied the criteria was input. The third was an experiment with directional control errors, and only the α values that satisfied the criteria were used.

Figure 8. Sensor setup in pool water.

6. Results

A. Threshold Measurement

The first data collected were the measurements of the threshold with variations in L at 2, 3.5, and 5 m, as shown in Figures 9, 10, and 11, respectively. The target was pulled by an electric motor at a constant speed of 1 m/s to make it pass by all four sensors. Wave ripples from the target propagated and hit the accelerometer, and each sensor sampled the magnitude of the acceleration on the vertical axis of the accelerometer every 28 ms. The acceleration measurements were obtained from the vertical axis only because it was the most affected by wave ripples. The magnitudes of the acceleration and timing of the event are depicted on the x and y axes, respectively, in Figures 9–11. As the figures show, when no target wave ripples were detected, the acceleration value of the four sensors was 0 m/s^2. Conversely, when target wave ripples occurred, the acceleration value was greater than or equal to 0.096 m/s^2. Therefore, the threshold value was obtained at 0.096 m/s^2.

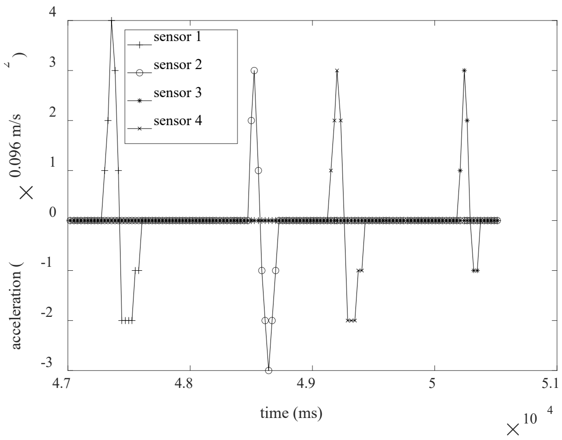

Figure 9. Threshold measurement for $L = 2$ m.

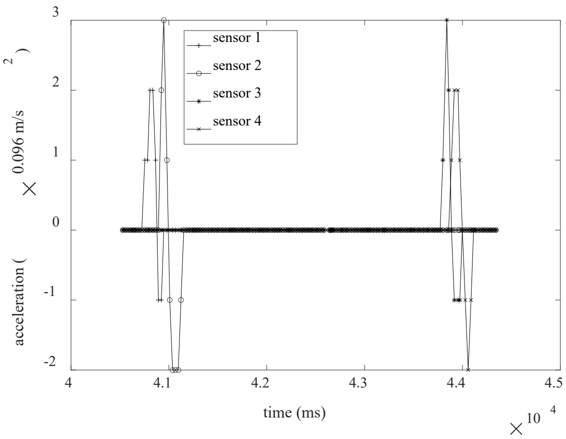

Figure 10. Threshold measurement for $L = 3.5$ m.

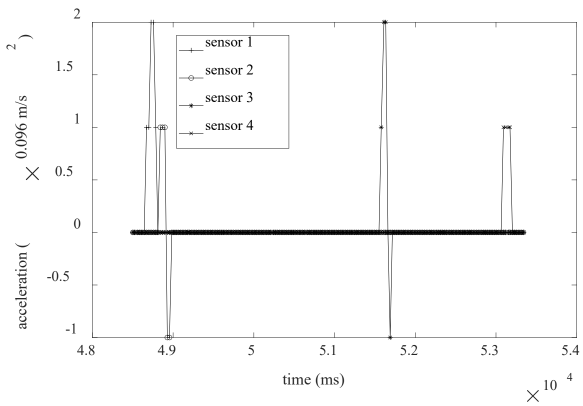

Figure 11. Threshold measurement for $L = 5$ m.

B. Data Acquisition

The data acquisition for the x and y axes was conducted by combining variations of the three parameters: $L = 2, 3.5, \text{and}\ \ 5$ m, $v = 1, 2, \text{and}\ \ 3$ m/s, and $\alpha =\ 80^0$, 90^0, and 100^0. Therefore, the total combination of the values of these parameters was 27, and each combination was conducted 5 times.

B.1. Estimation of the Target's Speed and Direction

Although the estimation of the target's velocity and direction was not the main objective of this study, the speed and direction were inputs for the estimation of x and y coordinates. Therefore, an evaluation of the estimated velocity and direction was important. First, the evaluation of the estimated speed was distinguished based on three different actual speeds, i.e., 1, 2, and 3 m/s (Figure 12). Each speed was obtained 45 times with various combinations of L and α. At the actual speed of 1 m/s, the estimated minimum and maximum velocities were 0.85 and 1.65 m/s, respectively. At 2 m/s, the estimated minimum and maximum speeds were 1.69 and 2.63 m/s, respectively. At 3 m/s, the estimated minimum and maximum speeds were 2.6 and 3.83 m/s, respectively. Second, the estimated direction was differentiated based on three actual directions, i.e., 80°, 90°, and 100° (Figure 13). Each direction was obtained by collecting 45 data points with various combinations of L and v. At the actual direction of 80°, the estimated minimum and maximum directions were 83.5° and 93.32°, respectively. At 90°, the estimated minimum and maximum directions were 81.96° and 96.23°, respectively. At 100°, the estimated minimum and maximum directions are 88° and 97.13°, respectively. The speed and direction estimation errors were caused by the target's wave ripples propagating at different speeds, resulting in the timestamps recorded by the sensor not being on time.

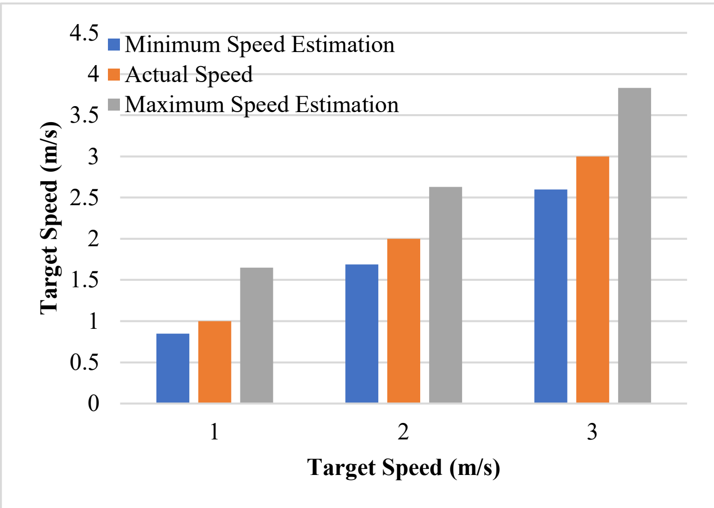

Figure 12. Target speed estimation.

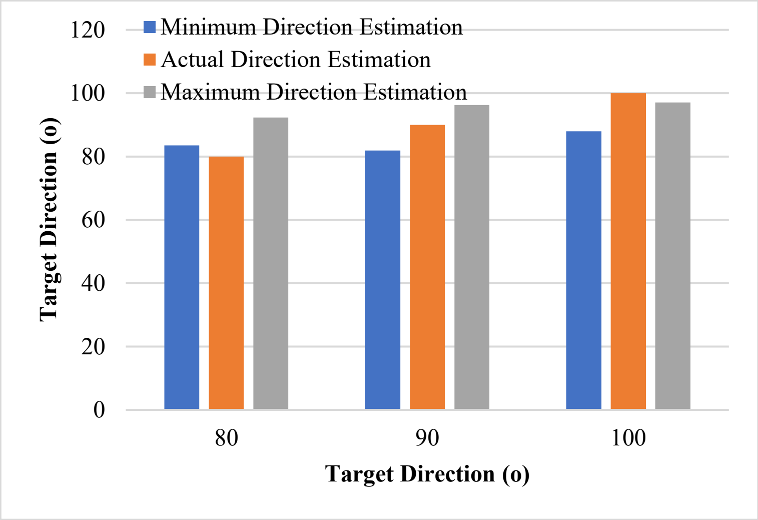

Figure 13. Target direction estimation.

B.2. MAE of x and y axes

The MAE calculations for the x and y axes were evaluated at the lengths $L = 2, 3.5$, and 5 m (Figure 14); the MAE size increased with increasing L. The solid and dashed lines indicate the MAE on the x- and y-axes, respectively. Closer to the solid line, the MAEs were 0.56, 1.03, and 1.60 m at the sensor distances of 2, 3.5, and 5 m, respectively. On the dashed line, the MAEs were 0.25, 0.72, and 1 m at sensor distances of 2, 3.5, and 5 m, respectively. We observed that the greater the distance between sensors, the longer the wave ripple took owing to the farther distance traveled. The farther the distance, the weaker the wave ripple magnitude of the target detected by the sensors. The interesting result in Figure 16 is that the MAE on the x-axis was always greater than that in the y. This phenomenon can be explained using the Abbe error principle, for which the directional error causes errors on the x and y axes [45] [46]. A comparison of the amount of error for the x and y axes is described in Section 5.2.3.

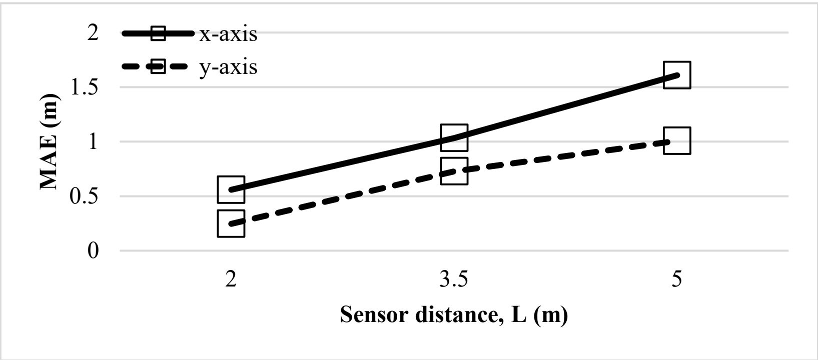

Figure 14. MAE for x- and y-axes versus sensor distance.

B.3. Error Explanation of x Versus y-Axes

The errors on the x= and y-axes can be explained using the actual direction variable, α. If $|\Delta\alpha|$ is the magnitude of the absolute deviation angle to the actual direction, then the estimated direction ($\hat{\alpha}$) being affected by $|\Delta\alpha|$ is

$$\hat{\alpha} = \alpha + |\Delta\alpha|. \quad (33)$$

The use of absolute values on $|\Delta\alpha|$ indicates the fact that the deviation consists of negative and positive deviations. If $S(x_\alpha, y_\alpha)$ and $T(x_{\hat{\alpha}}, y_{\hat{\alpha}})$ are the actual and estimated coordinates, respectively, then the absolute deviation of the x-axis as a function of α and $\Delta\alpha$ is

$$\Delta x = |x_\alpha - x_{\hat{\alpha}}|$$
$$= |\cos\alpha - \cos(\alpha + |\Delta\alpha|)|. \quad (34)$$

The absolute deviation of the y-axis is

$$\Delta y = |y_\alpha - y_{\hat{\alpha}}|$$
$$= |\sin\alpha - \sin(\alpha + |\Delta\alpha|)|. \quad (35)$$

For $\alpha = 90°$, (34), and (35) can be simplified as $\Delta x = \sin|\Delta\alpha|$ and $\Delta y = 1 - \cos|\Delta\alpha|$, respectively. Moreover, to prove $\Delta x \geq \Delta y$, the range of $\Delta\alpha$ can be determined as

$$\Delta x \geq \Delta y$$
$$\sin\Delta\alpha \geq 1 - \cos\Delta\alpha$$
$$\sin\Delta\alpha + \cos\Delta\alpha - 1 \geq 0. \quad (36)$$

(36) holds if $\Delta\alpha$ falls within -90° $\leq \Delta\alpha \leq$ 90°. The deviation graphs of Δx (solid) and Δy (dashed) against the angle deviation ($\Delta\alpha$) is shown in Figure 15. The condition $\Delta x \geq \Delta y$ holds for $|\Delta\alpha| \leq 90°$, while the condition $\Delta x < \Delta y$ holds for $|\Delta\alpha| > 90°$. Referring to Figure 15, for α =90°, $\Delta\alpha$ has a range of angle deviation between $-1.96° \leq \Delta\alpha \leq 6.23°$, where the range is still narrower than the required range. Thus, the phenomenon of the deviation of the axis Δx is greater than that of the axis Δy.

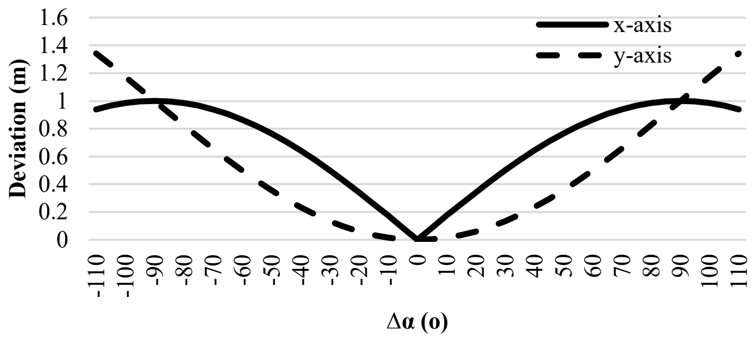

Figure 15. Deviation of *x* and *y*-axes around $\alpha = 90°$.

B.4. MAE with Error Control

As discussed in Section 6.2.1, errors occurred in the estimation of speed and direction. Since the estimation of the x- and y-axes was a function of velocity and direction, any error in estimating the velocity and direction caused errors in the estimation of the x- and y-axes. Therefore, controlling the speed and direction errors was important. Error control was conducted by limiting the error to the estimated speed and direction. The error control was measured using the MAE for the x- and y-axes. The MAEs were calculated using three experimental scenarios, i.e., no error control, speed error control, and direction error control (Figure 16). In the scenarios of speed and direction error control, the maximum error limits of both were 10%. The solid and dashed lines in Figure 18 indicate the MAE of the x and y axes, respectively. Closer to the solid lines, the direction error control scenario produced the smallest MAE compared with the speed error control and no error control scenarios. For example, at L 5 m, the MAEs for no error control, speed error control, and direction error control were 1.26, 0.87, and 0.5 m, respectively. The same phenomenon also occurred on the dashed lines, for which the direction error control indicated the smallest MAE value. These results implied that the direction error control was better than the speed error control.

After we observed that the direction error control can significantly reduce the MAE, the subsequent experiment aimed to observe the effect of direction error control, which was divided into a maximum of 10%, 7.5%, and 5% (Figure 17). The solid and dotted lines show the MAE on the x- and y-axes, respectively. Closer to the solid and dotted lines with the triangle marker, the maximum 5% direction error control resulted in the smallest MAE. This result corresponded with the expectation that the smaller the direction error, the smaller the estimated error on the x- and y-axes.

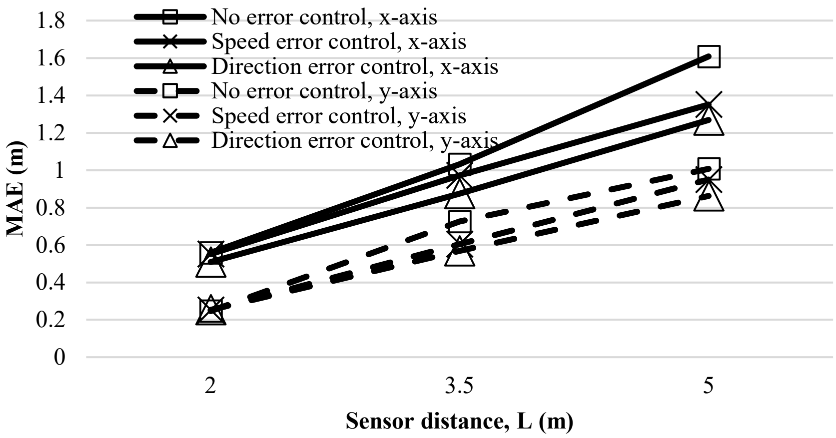

Figure 16. *MAE* of x and y-axes with speed and direction error controls.

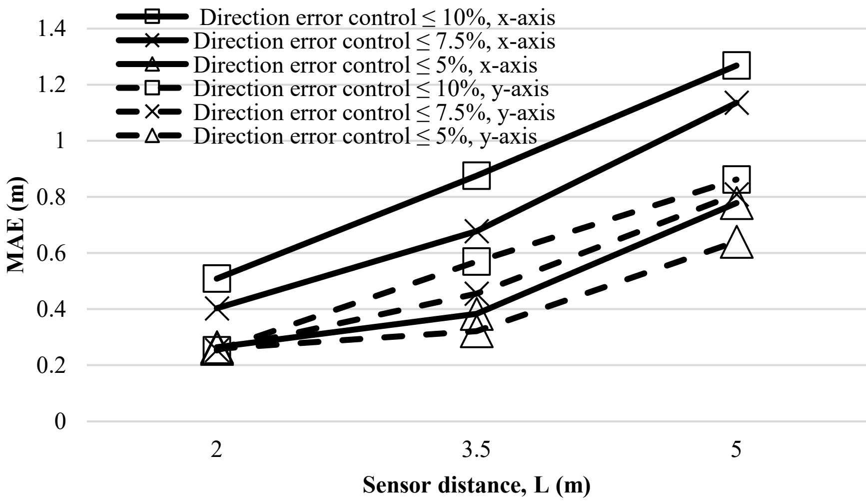

Figure 17. *MAE* of x and y-axes with various direction error controls: $\leq 10\%, \leq 7.5\%,$ and $\leq 5\%$.

7. Discussion

The main objective of this research was to detect the location of moving targets on a water surface. The proposed solution is an algorithm that can calculate the coordinates of the target, i.e., x- and y-axes. The algorithm was implemented in the target detection system, and its performance was measured using the MAE parameter. The evaluation of MAE on the distance between sensors indicated that the greater the distance between sensors, the greater the MAE. This result was not surprising because as the distance between the sensors increases, the wave magnitude generated by the moving target decreased. This implied that a tighter sensor deployment in the region of interest can increase the detection accuracy of the target location.
The interesting result from this study was the x-axis MAE, which was always greater than that of the y-axis. This phenomenon is explained in Section 6. 2. 3 based on the principle of the Abbe error. Moreover, this phenomenon has potential benefits in explaining the problem of measurement accuracy in other research topics, such as a parallel coordinate measuring machine (PCMM).

Additionally, this study confirmed that errors occurring in the estimation of the target speed and direction can cause errors in the estimation of the target location. To minimize location estimation errors, speed and direction error control is necessary. The results indicated that direction error control has a greater effect than speed error control in reducing the MAE on the x- and y-axes. These results suggest that increasing the accuracy of detecting the location of moving targets could focus on mitigating errors in a particular direction. The mitigation of the direction estimation error, based on (5), can focus on increasing the timestamp accuracy of each sensor.

The limitation of this research is that the experiment was conducted on a relatively calm water surface to enable the sensors to easily recognize the existence of the target based on the threshold magnitude of the water waves. Experiments on dynamic water surfaces, such as at sea, will challenge sensors in recognizing the presence of a target. Sensors will require to use another method, such as the water wave spectrum threshold. In addition to these limitations, the proposed algorithm for calculating the target location can be applied directly. Thus, locating moving targets in a dynamic water environment using the water wave spectrum threshold is still an open problem.

8. Conclusions

The purpose of this research was to detect the location of a moving target on a calm water surface using a wireless sensor network (WSN). This study proposed an algorithm that can calculate the target coordinates. The experimental results indicate that the proposed algorithm can locate moving targets with the smallest mean average error of 0.25 m. This research has contributed to the topic of detecting moving targets using WSNs by determining the location of these targets. The more attributes of the target are known, the more comprehensive the detection system will be. Subsequent research will involve detecting the target location on a dynamic water surface and determining its correlation with the MAE.

Author Contributions: Conceptualization, methodology, formal analysis, investigation, writing, visualization, funding acquisition A.S.A.; software, data curation T.S.F.

Acknowledgments: This research was funded by Universitas Indonesia under Program PUTI Q2 2020 grant number NKB-1719/UN2.RST/HKP.05.00/2020.

Conflicts of Interest: The authors declare no conflicts of interest.

9. References

[1]. J. Aponte-Luis, J. A. Gómez-Galán, F. Gómez-Bravo, M. Sánchez-Raya, J. Alcina-Espigado, and P. M. Teixido-Rovira, "An Efficient Wireless Sensor Network for Industrial Monitoring and Control," *Sensors (Basel, Switzerland)*, vol. 18, no. 1, Jan. 2018, doi: 10.3390/S18010182.

[2]. H. M. Jawad, R. Nordin, S. K. Gharghan, A. M. Jawad, and M. Ismail, "Energy-Efficient Wireless Sensor Networks for Precision Agriculture: A Review," *Sensors 2017, Vol. 17, Page 1781*, vol. 17, no. 8, p. 1781, Aug. 2017, doi: 10.3390/S17081781.

[3]. S. Kumar, S. Duttagupta, V. P. Rangan, and M. V. Ramesh, "Reliable network connectivity in wireless sensor networks for remote monitoring of landslides," *Wireless Networks 2019 26:3*, vol. 26, no. 3, pp. 2137–2152, Jun. 2019, doi: 10.1007/S11276-019-02059-7.

[4]. A. B. Noel, A. Abdaoui, T. Elfouly, M. H. Ahmed, A. Badawy, and M. S. Shehata, "Structural Health Monitoring Using Wireless Sensor Networks: A Comprehensive Survey," *IEEE Communications Surveys and Tutorials*, vol. 19, no. 3, pp. 1403–1423, Jul. 2017, doi: 10.1109/COMST.2017.2691551.

[5]. G. Xu, Y. Shi, X. Sun, and W. Shen, "Internet of Things in Marine Environment Monitoring: A Review," *Sensors 2019, Vol. 19, Page 1711*, vol. 19, no. 7, p. 1711, Apr. 2019, doi: 10.3390/S19071711.

[6]. G. Xu, W. Shen, and X. Wang, "Applications of Wireless Sensor Networks in Marine Environment Monitoring: A Survey," *Sensors 2014, Vol. 14, Pages 16932-16954*, vol. 14, no. 9, pp. 16932–16954, Sep. 2014, doi: 10.3390/S140916932.

[7]. M. Rao, N. K. Kamila, and K. V. Kumar, "Underwater wireless sensor network for tracking ships approaching harbor," *International Conference on Signal Processing, Communication, Power and Embedded System, SCOPES 2016 - Proceedings*, pp. 1872–1876, Jun. 2017, doi: 10.1109/SCOPES.2016.7955771.

[8]. A. Sharma and S. Chauhan, "Sensor Fusion for Distributed Detection of Mobile Intruders in Surveillance Wireless Sensor Networks," *IEEE Sensors Journal*, vol. 20, no. 24, pp. 15224–15231, Dec. 2020, doi: 10.1109/JSEN.2020.3009828.

[9]. W. Wang, H. Huang, Q. Li, F. He, and C. Sha, "Generalized Intrusion Detection Mechanism for Empowered Intruders in Wireless Sensor Networks," *IEEE Access*, vol. 8, pp. 25170–25183, 2020, doi: 10.1109/ACCESS.2020.2970973.

[10]. S. K. Mohapatra, P. K. Sahoo, and S. L. Wu, "Big data analytic architecture for intruder detection in heterogeneous wireless sensor networks," *Journal of Network and Computer Applications*, vol. 66, pp. 236–249, May 2016, doi: 10.1016/J.JNCA.2016.03.004.

[11]. Z. Wang, E. Bulut, and B. K. Szymanski., "Distributed energy-efficient target tracking with binary sensor networks," *ACM Transactions on Sensor Networks (TOSN)*, vol. 6, no. 4, pp. 1–32, Jul. 2010, doi: 10.1145/1777406.1777411.

[12]. M. Arik and O. B. Akan, "Collaborative mobile target imaging in UWB wireless radar sensor networks," *IEEE Journal on Selected Areas in Communications*, vol. 28, no. 6, pp. 950–961, Aug. 2010, doi: 10.1109/JSAC.2010.100820.

[13]. T. He *et al.*, "Energy-efficient surveillance system using wireless sensor networks," *MobiSys 2004 - Second International Conference on Mobile Systems, Applications and Services*, pp. 270–283, 2004, doi: 10.1145/990064.990096.

[14]. P. Dutta, M. Grimmer, A. Arora, S. Bibykt, and D. Culler, "Design of a wireless sensor network platform for detecting rare, random, and ephemeral events," *2005 4th International Symposium on Information Processing in Sensor Networks, IPSN 2005*, vol. 2005, pp. 497–502, 2005, doi: 10.1109/IPSN.2005.1440983.

[15]. H. Zhu, Y. Zhu, M. Li, and L. M. Ni, “HERO: Online Real-Time Vehicle Tracking in Shanghai,” pp. 942–950, Jun. 2008, doi: 10.1109/INFOCOM.2008.147.

[16]. M. F. Duarte and Y. H. Hu, “Vehicle classification in distributed sensor networks,” *Journal of Parallel and Distributed Computing*, vol. 64, no. 7, pp. 826–838, Jul. 2004, doi: 10.1016/J.JPDC.2004.03.020.

[17]. AroraA. *et al.*, “A line in the sand,” *Computer Networks: The International Journal of Computer and Telecommunications Networking*, vol. 46, no. 5, pp. 605–634, Dec. 2004, doi: 10.1016/J.COMNET.2004.06.007.

[18]. B. Bunin, A. Sutin, G. Kamberov, H.-S. Roh, B. Luczynski, and M. Burlick, “Fusion of acoustic measurements with video surveillance for estuarine threat detection,” *Optics and Photonics in Global Homeland Security IV*, vol. 6945, p. 694514, Apr. 2008, doi: 10.1117/12.779176.

[19]. E. M. Carapezza, J. Butman, I. Babb, and A. Bucklin, “Sustainable coastal sensor networks: technologies and challenges,” *Unattended Ground, Sea, and Air Sensor Technologies and Applications X*, vol. 6963, p. 696309, Apr. 2008, doi: 10.1117/12.786636.

[20]. H. Kdouh, G. Zaharia, C. Brousseau, H. Farhat, G. Grunfelder, and G. El, “Application of Wireless Sensor Network for the Monitoring Systems of Vessels,” in *Wireless Sensor Networks - Technology and Applications*, InTech, 2012. doi: 10.5772/48276.

[21]. H. Luo, K. Wu, Z. Guo, L. Gu, and L. M. Ni, “Ship Detection with Wireless Sensor Networks,” *IEEE Transactions on Parallel and Distributed Systems*, vol. 23, no. 7, pp. 1336–1343, Jul. 2012, doi: 10.1109/TPDS.2011.274.

[22]. H. Luo, K. Wu, and F. Hong, “Ocean Barrier: A Floating Intrusion Detection Ocean Sensor Networks,” in *2016 12th International Conference on Mobile Ad-Hoc and Sensor Networks (MSN)*, Dec. 2016, pp. 390–394. doi: 10.1109/MSN.2016.071.

[23]. M. Rao and N. K. Kamila, “Tracking intruder ship in wireless environment,” *Human-centric Computing and Information Sciences*, vol. 7, no. 1, p. 14, Dec. 2017, doi: 10.1186/s13673-017-0095-4.

[24]. S. L., N. F., and P. W., “Target Tracking for Sensor Networks,” *ACM Computing Surveys (CSUR)*, vol. 49, no. 2, Jun. 2016, doi: 10.1145/2938639.

[25]. N. H. Nguyen, “Optimal Geometry Analysis for Target Localization with Bayesian Priors,” *IEEE Access*, vol. 9, pp. 33419–33437, 2021, doi: 10.1109/ACCESS.2021.3056440.

[26]. E. L. Souza, A. Campos, and E. F. Nakamura, “Tracking targets in quantized areas with wireless sensor networks,” *Proceedings - Conference on Local Computer Networks, LCN*, pp. 235–238, 2011, doi: 10.1109/LCN.2011.6115197.

[27]. L. Shi and J. Tan, “Distributive target tracking in sensor networks with a Markov random field model,” *2009 IEEE/RSJ International Conference on Intelligent Robots and Systems, IROS 2009*, pp. 854–859, Dec. 2009, doi: 10.1109/IROS.2009.5354756.

[28]. R. Boutaba, N. Achir, M. St-Hilaire, and E. F. Nakamura, “Planning and Deployment of Wireless Sensor Networks:,” *http://dx.doi.org/10.1155/2014/198139*, vol. 2014, Jan. 2014, doi: 10.1155/2014/198139.

[29]. S. Zhao, B. M. Chen, and T. H. Lee, “Optimal deployment of mobile sensors for target tracking in 2D and 3D spaces,” *IEEE/CAA Journal of Automatica Sinica*, vol. 1, no. 1, pp. 24–30, Jan. 2014, doi: 10.1109/JAS.2014.7004616.

[30]. S. Zhao, B. M. Chen, and T. H. Lee, “Optimal Sensor Placement for Target Localization and Tracking in 2D and 3D,” Oct. 2012, Accessed: Sep. 20, 2021. [Online]. Available: http://arxiv.org/abs/1210.7397

[31]. S. Martínez and F. Bullo, “Optimal sensor placement and motion coordination for target tracking,” *Automatica*, vol. 42, no. 4, pp. 661–668, Apr. 2006, doi: 10.1016/J.AUTOMATICA.2005.12.018.

[32]. Y. Oshman and P. Davidson, “Optimization of observer trajectories for bearings-only target localization,” *IEEE Transactions on Aerospace and Electronic Systems*, vol. 35, no. 3, pp. 892–902, 1999, doi: 10.1109/7.784059.

[33]. J. Ousingsawat and M. E. Campbell, “Optimal Cooperative Reconnaissance Using Multiple Vehicles,” *https://doi.org/10.2514/1.19147*, vol. 30, no. 1, pp. 122–132, May 2012, doi: 10.2514/1.19147.

[34]. L. Cheng, C. Wu, Y. Zhang, H. Wu, M. Li, and C. Maple, “A Survey of Localization in Wireless Sensor Network:,” *International Journal of Distributed Sensor Networks*, vol. 2012, no. 12, Dec. 2012, doi: 10.1155/2012/962523.

[35]. K. Doğançay and H. Hmam, “Optimal angular sensor separation for AOA localization,” *Signal Processing*, vol. 88, no. 5, pp. 1248–1260, May 2008, doi: 10.1016/J.SIGPRO.2007.11.013.

[36]. N. H. Nguyen and K. Dogancay, “Optimal Geometry Analysis for Multistatic TOA Localization,” *IEEE Transactions on Signal Processing*, vol. 64, no. 16, pp. 4180–4193, Aug. 2016, doi: 10.1109/TSP.2016.2566611.

[37]. K. W. K. Lui and H. C. So, “A study of two-dimensional sensor placement using time-difference-of-arrival measurements,” *Digital Signal Processing*, vol. 19, no. 4, pp. 650–659, Jul. 2009, doi: 10.1016/J.DSP.2009.01.002.

[38]. A. N. Bishop and P. Jensfelt, “An optimality analysis of sensor-target geometries for signal strength based localization,” *ISSNIP 2009 - Proceedings of 2009 5th International Conference on Intelligent Sensors, Sensor Networks and Information Processing*, pp. 127–132, 2009, doi: 10.1109/ISSNIP.2009.5416784.

[39]. L. Cheng, C. D. Wu, and Y. Z. Zhang, "Indoor robot localization based on wireless sensor networks," *IEEE Transactions on Consumer Electronics*, vol. 57, no. 3, pp. 1099–1104, Aug. 2011, doi: 10.1109/TCE.2011.6018861.

[40]. N. H. Nguyen and K. Dogangay, "Optimal sensor-target geometries for Doppler-shift target localization," *2015 23rd European Signal Processing Conference, EUSIPCO 2015*, pp. 180–184, Dec. 2015, doi: 10.1109/EUSIPCO.2015.7362369.

[41]. N. H. Nguyen and K. Doƚançay, "Optimal sensor placement for Doppler shift target localization," *IEEE National Radar Conference - Proceedings*, vol. 2015-June, no. June, pp. 1677–1682, Jun. 2015, doi: 10.1109/RADAR.2015.7131268.

[42]. Y. Wang, X. Wang, D. Wang, and D. P. Agrawal, "Range-free localization using expected hop progress in wireless sensor networks," *IEEE Transactions on Parallel and Distributed Systems*, vol. 20, no. 10, pp. 1540–1552, 2009, doi: 10.1109/TPDS.2008.239.

[43]. F. Gustafsson and F. Gunnarsson, "Localization based on observations linear in log range," *IFAC Proceedings Volumes*, vol. 41, no. 2, pp. 10252–10257, 2008, doi: 10.3182/20080706-5-KR-1001.01735.

[44]. X. Jin, S. Sarkar, A. Ray, S. Gupta, and T. Damarla, "Target detection and classification using seismic and PIR sensors," *IEEE Sensors Journal*, vol. 12, no. 6, pp. 1709–1718, 2012, doi: 10.1109/JSEN.2011.2177257.

[45]. S. R. Sleep, "An adaptive belief representation for target tracking using disparate sensors in Wireless Sensor Networks," in *Proceedings of the 16th International Conference on Information Fusion, FUSION 2013*, 2013, pp. 2073–2080.

[46]. K. R *et al.*, "A radar-enabled collaborative sensor network integrating COTS technology for surveillance and tracking," *Sensors (Basel, Switzerland)*, vol. 12, no. 2, pp. 1336–1351, Feb. 2012, doi: 10.3390/S120201336.

[47]. A. Oka and L. Lampe, "Distributed target tracking using signal strength measurements by a wireless sensor network," *IEEE Journal on Selected Areas in Communications*, vol. 28, no. 7, pp. 1006–1015, Sep. 2010, doi: 10.1109/JSAC.2010.100905.

[48]. M. Chiani, A. Giorgetti, M. Mazzotti, R. Minutolo, and E. Paolini, "Target detection metrics and tracking for UWB radar sensor networks," *Proceedings - 2009 IEEE International Conference on Ultra-Wideband, ICUWB 2009*, pp. 469–474, 2009, doi: 10.1109/ICUWB.2009.5288758.

[49]. Z. Wang, W. Lou, Z. Wang, J. Ma, and H. Chen, "A Novel Mobility Management Scheme for Target Tracking in Cluster-Based Sensor Networks," *Lecture Notes in Computer Science (including subseries Lecture Notes in Artificial Intelligence and*

Lecture Notes in Bioinformatics), vol. 6131 LNCS, pp. 172–186, 2010, doi: 10.1007/978-3-642-13651-1_13.

[50]. B. H. Liu, W. C. Ke, C. H. Tsai, and M. J. Tsai, “Constructing a message-pruning tree with minimum cost for tracking moving objects in wireless sensor networks is NP-complete and an enhanced data aggregation structure,” *IEEE Transactions on Computers*, vol. 57, no. 6, pp. 849–863, Jun. 2008, doi: 10.1109/TC.2008.22.

[51]. SinghJaspreet, KumarRajesh, MadhowUpamanyu, SuriSubhash, and CagleyRichard, “Multiple-Target Tracking With Binary Proximity Sensors,” *ACM Transactions on Sensor Networks (TOSN)*, vol. 8, no. 1, Aug. 2011, doi: 10.1145/1993042.1993047.

[52]. L. H. Yen, B. Y. Wu, and C. C. Yang, “Tree-based object tracking without mobility statistics in wireless sensor networks,” *Wireless Networks*, vol. 16, no. 5, pp. 1263–1276, Jul. 2010, doi: 10.1007/S11276-009-0201-2.

[53]. M. Mansouri and L. Khoukhi, “Secure quantized target tracking in wireless sensor networks,” *IWCMC 2011 - 7th International Wireless Communications and Mobile Computing Conference*, pp. 713–718, 2011, doi: 10.1109/IWCMC.2011.5982634.

[54]. E. Xu, Z. Ding, and S. Dasgupta, “Target tracking and mobile sensor navigation in wireless sensor networks,” *IEEE Transactions on Mobile Computing*, vol. 12, no. 1, pp. 177–186, 2013, doi: 10.1109/TMC.2011.262.

[55]. M. Aernouts, N. BniLam, R. Berkvens, and M. Weyn, “TDAoA: A combination of TDoA and AoA localization with LoRaWAN,” *Internet of Things*, vol. 11, p. 100236, Sep. 2020, doi: 10.1016/J.IOT.2020.100236.

[56]. Y. Sun, K. C. Ho, and Q. Wan, “Solution and Analysis of TDOA Localization of a Near or Distant Source in Closed Form,” *IEEE Transactions on Signal Processing*, vol. 67, no. 2, pp. 320–335, Jan. 2019, doi: 10.1109/TSP.2018.2879622.

[57]. A. Boukerche, H. A. B. F. Oliveira, E. F. Nakamura, and A. A. F. Loureiro, “Localization systems for wireless sensor networks,” *IEEE Wireless Communications*, vol. 14, no. 6, pp. 6–12, Dec. 2007, doi: 10.1109/MWC.2007.4407221.

[58]. M. Rao and N. K. Kamila, “Tracking intruder ship in wireless environment,” *Human-centric Computing and Information Sciences*, vol. 7, no. 1, pp. 1–26, Dec. 2017, doi: 10.1186/s13673-017-0095-4.

[59]. F. Ursell, “On Kelvin’s ship-wave pattern,” *Journal of Fluid Mechanics*, vol. 8, no. 3, pp. 418–431, 1960, doi: 10.1017/S0022112060000700.

[60]. R. Leach, “Abbe Error/Offset,” in *CIRP Encyclopedia of Production Engineering*, Springer Berlin Heidelberg, 2014, pp. 1–4. doi: 10.1007/978-3-642-35950-7_16793-1.

[61]. P.-H. Hu, C.-W. Yu, K.-C. Fan, X.-M. Dang, and R.-J. Li, “Error Averaging Effect in Parallel Mechanism Coordinate Measuring Machine,” *Applied Sciences*, vol. 6, no. 12, p. 383, Nov. 2016, doi: 10.3390/app6120383.

Ajib Setyo Arifin received the Bachelor in Electrical Engineering and Master’s Degree from the Universitas Indonesia, in 2009 and 2011, respectively. He has got the PhD. degree in Telecommunications in 2015 from the Keio University, Japan. He is an associate professor at Universitas Indonesia. He was a head of telecommunication laboratory in Department of Electrical Engineering. His research areas include Wireless Sensor Networks, Wireless Communication, and signal processing for communication. His Orcid id is 0000-0002-4827-6642 and email id is ajib@eng.ui.ac.id

Teguh Samudra Firdaus received the Bachelor in Electrical Engineering from the Universitas Indonesia in 2017. His research is Wireless Sensor Networks. He works in telecommunication company. His email id is samudraasta@gmail.com.